0.13µm SiGe BiCMOS W-Band Low-Noise Amplifier for Passive Imaging Systems

Berke Gungor, Esref Turkmen, Melik Yazici, Mehmet Kaynak*, Yasar Gurbuz
Faculty of Engineering and Natural Sciences, Sabanci University, Orhanli, Tuzla, 34956, Istanbul, Turkey
*IHP Microelectronics, Im Technologiepark, 25, 15236, Frankfurt (Oder), Germany
yasar@sabanciuniv.edu

***Abstract*— This paper presents a W-band LNA implemented in 0.13µm SiGe BiCMOS technology. The designed LNA has a peak gain of 20.5dB at 80GHz with a 3-dB bandwidth greater than 25GHz. The simulated noise figure (NF) is lower than 6.2 dB across the entire W-band with a minimum of 5 dB at 93 GHz. The LNA has input P_{1dB} of -16dBm at 94 GHz. The total quiescent DC power consumption of the designed LNA is 16.6mW with a 1.3V supply voltage. Inductors were utilized in matching networks instead of transmission lines to reduce the chip area. The total integrated circuit occupies an area of 0.33 mm², and the effective chip area is 0.2mm², excluding the pads. Simulation results indicate that the designed LNA is suitable to be used in a radiometer that has NETD smaller than 0.5 K.**

***Index Terms*—LNA, W-band, passive imaging, millimeter-wave, silicon germanium, BiCMOS;**

I. Introduction

Over the recent years, the significant advancements in the silicon-based technologies enabled process technologies such as SiGe BiCMOS to reach high f_t/f_{max} values and made them comparable with the traditional III-V technologies in the millimeter-wave (mmW) spectrum (30-300GHz). Such developments in the cheaper silicon-based technologies lead significant growth in mmW applications. Especially the low atmospheric attenuation window in the W-band frequencies (75-110GHz) made it favorable for various sensing applications such as passive imaging [1], automotive radars [2] and high-speed communication [3]. Common to almost all the wireless receivers, aforementioned applications all require the use of a low-noise amplifier (LNA) with high gain to suppress the noise of the following stages while contributing minimal noise to the system with a low noise figure (NF).

Passive imaging systems or radiometers pick up the mmW radiation emitted from the targeted objects. Total power radiometer (TPR) is the one of the most commonly used radiometer architecture in mmW passive imaging systems. In a typical TPR front end, the antenna is followed immediately by an LNA and then a power detector. The radiometer sensitivity, which is also termed as noise equivalent temperature difference (NETD), for a TPR is given by equation (1):

$$\Delta T = T_S \sqrt{\frac{1}{B\tau} + \left(\frac{\Delta G}{G}\right)} \qquad (1)$$

where B is the 3-dB bandwidth, τ is the back-end integration time, T_S is the system noise temperature and ΔG/G describes the LNA gain fluctuation [4].

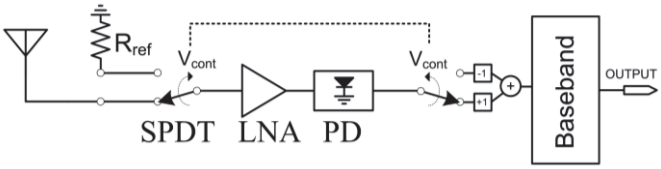

Fig. 1: Simplified block diagram of a Dicke type radiometer.

In a TPR, gain fluctuation $(\Delta G/G)$ of the LNA is a serious detriment to the NETD of the system, as also presented in equation (1). This gain fluctuation term can be eliminated using the Dicke radiometer architecture [5]. In the Dicke type radiometers, the gain fluctuation term is eliminated by periodic calibration of the system with the use of an SPDT switch at the cost of slightly increased overall system NF and a factor of 2 on the equation due to halved observation time. NETD for Dicke type radiometer is given in equation (2) [6].

$$\Delta T = \frac{2T_S}{\sqrt{B\tau}} \qquad (2)$$

For passive imaging applications, NETD less than 1 K is required to be suitable for imaging [7]. As can be seen from equation (2), it is critical to design the LNA with high bandwidth, along with low noise and high gain in order to achieve a desired NETD performance.

This paper presents a high bandwidth W-band four-stage common-emitter LNA designed using IHP's 0.13-µm SiGe BiCMOS technology (SG13G2). Section II describes the LNA design, starting with the considerations regarding the topology selection and followed by the design process of the four-stage LNA. Finally, the simulation results are reported in Section III and compared with other published W-band LNAs.

II. LNA Design

A. Topology Selection

Fig. 1 shows the simplified diagram of a typical Dicke type radiometer that consists of an antenna followed by an SPDT switch, an LNA, and a power detector. As previously mentioned in Section I, a radiometer system has to achieve a NETD performance < 1K to be suitable for imaging. Consequently, an NETD performance of <0.5K for the system is chosen as the goal while determining the required specifications of the LNA. A sample calculation using equation (2) shows that a radiometer system with a total NF of 13 dB, 20 GHz RF bandwidth and τ of 30ms yields NETD less than 0.5K. Several W-band SPDT switches are reported [1], [8] in SiGe with insertion losses (IL)

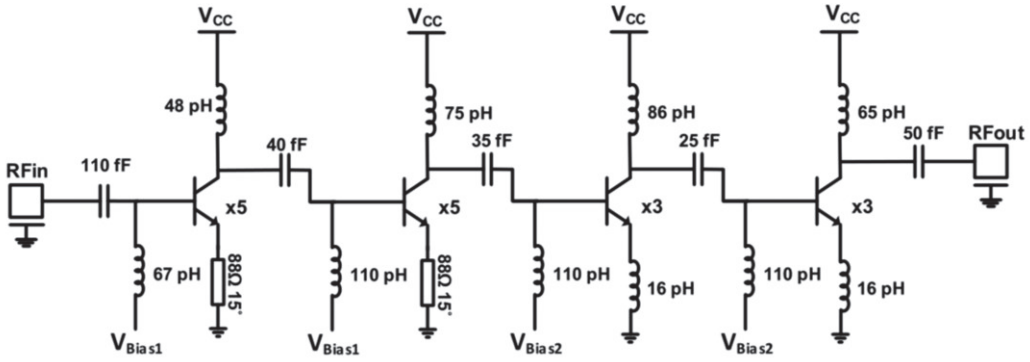

Fig. 3: LNA schematic (biasing not shown, and electrical lengths are given for 94GHz).

of around 2 dB. In addition, several studies present W-band power detectors in SiGe with noise equivalent powers (NEP) of around 0.5 pW/Hz$^{1/2}$ [9], [10]. Using the IL and NF values from the reported works to calculate the overall system NF shows that approximately 18dB gain and 5dB NF for the LNA is required for the NETD performance better than 0.5K.

There are several topologies that are commonly used to build an LNA. The most common of those topologies are the common emitter and cascode topologies. It is important to consider the potential tradeoffs while choosing the topology during the design of an LNA. Fig. 2 shows the maximum available gain and minimum NF of a single common-emitter stage for the IHP's npn13G2 device (2.7 µm emitter length). This figure also shows the minimum noise figure of the cascaded four stage for the common emitter configuration.

Even though single cascode stage typically provides higher gain, it has a slightly higher noise figure and higher power consumption than the CE. Also in the CE configuration, due to the low isolation of a CE stage, output matching network also affects the input matching network. This feature of the CE configuration turns into an advantage in the design of an LNA for passive imaging applications as it allows wideband matching

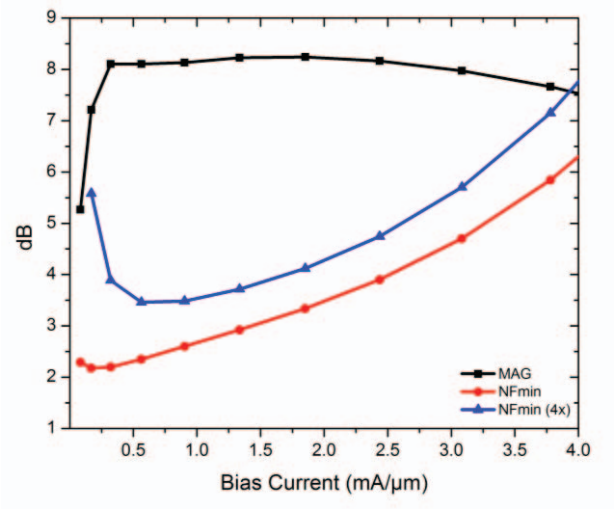

Fig. 2: Maximum available gain and minimum noise figure for the common emitter LNA stage. Four stage cascaded NF is also shown.

at the input, output and the inter-stages. Finally, the lower supply voltage requirement of the CE stage makes it more suitable for integration into low-power passive imaging systems. Due to the aforementioned advantages, common emitter topology was preferred over cascode configuration.

B. Circuit Design

Keeping the previously mentioned design considerations in mind, LNA was designed in four cascaded degenerated CE stages. The simplified schematic is shown in Fig. 3. First two stages were optimized for minimum NF with a compromise in maximum available gain (MAG). While optimizing the first stage of a cascaded LNA topology for minimum NF is common practice, the second stage was also optimized for minimum noise since the available gain of the first CE stage is not high enough to suppress the noises of the following stages. The optimum collector current was found to be 0.4mA for the unit emitter size. The number of the transistor was optimized to be x5 to enable simultaneous noise and power matching [11]. Parasitic capacitances of the RF pads were taken into account in simultaneous noise and power matching. A metal-insulator-metal (MIM) capacitor of 110 fF was used as a DC blocking capacitor, and it was taken into account in the input impedance matching. 88 Ω, 15° transmission lines were used in the first two stages for the emitter degeneration to set the real part of the input impedance to 50Ω. The emitter degeneration transmission lines were all implemented as microstrip transmission lines (MSLs) with a TopMetal2-Metal1 configuration.

For third and fourth stages, a higher bias current was chosen for higher gain with a trade-off in noise figure. 3x transistor size and a bias current of 1.7mA/um is chosen. All of the capacitors were implemented as metal-insulator-metal (MIM) capacitors, except the interstage capacitor of 25fF between 3rd and 4th stages, which was implemented as metal-oxide-metal. RF pads were custom designed using the TM2 layer with the dimensions 40 x 60 µm^2 to keep the parasitic capacitances as minimum as possible, and also the edges were trimmed to further decrease the parasitic capacitance.

The transistors were biased using simple R-C sections, 450fF MIM shunt capacitors were used as RF grounding after the inductors on the bias lines. 2pF MIM shunt capacitances were used to improve low-frequency stability and improve the

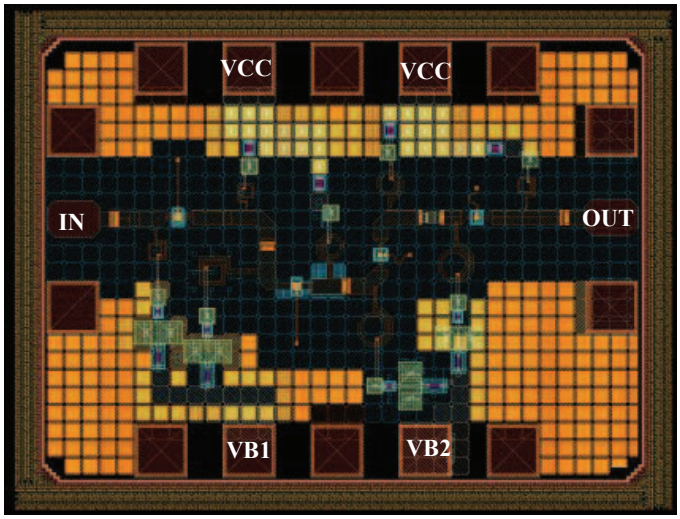

Fig. 4: Full layout of the LNA. Chip area is 670µm x 500µm^2 including the pads, 550µm x 320µm^2 excluding the pads.

isolation between the stages. 20 Ω silicide resistors were added between the two capacitors to avoid adding up the parasitic effects which would result in a significant degradation in the total self-resonance frequency of the bias network.

Use of inductors was preferred to transmission lines in the input and output matching networks as well as the inter-stages to avoid larger chip area. All inductors were designed using TM2 and TM1 layers. Octagonal spiral geometry was utilized to achieve high Q-factor inductors while some of the inductors were realized with rectangular spiral geometry to intentionally lower the Q-factor for matching purposes. All inductors were modeled and simulated using Sonnet.

III. Simulation Results

The LNA is implemented in the IHP's 0.13µm SiGe BiCMOS technology, SG13G2, featuring HBTs with $f_t/f_{max}/BV_{CEO}$ of 300/500GHz/1.6V. The back-end-of-line (BEOL) of the process consists of seven metallization layers, five thin (M1-M5) and two thick layers (TM2-TM1) for high-quality on-chip inductor and transmission line designs. Metal-insulator-metal (MIM) capacitors were formed between M5 and TM1 layers with a separate insulator layer in between. [12]

The layout of the LNA is shown in Fig. 4. The total integrated circuit occupies an area of 0.33 mm^2, and the effective chip area is 0.2mm^2, excluding the pads. The LNA draws the total of 12.8mA of current from 1.3V supply, and the total quiescent power consumption is 16.6 mW. In addition, the bias voltages of the third and fourth stages could be adjusted to reduce quiescent power consumption to 10mW with a small trade-off in gain and overall matching. Full layout EM simulations were performed in ADS Momentum excluding the bias lines and fillers. RF pads were also simulated in ADS Momentum individually during the schematic design to account for its parasitic capacitance as previously mentioned.

The simulated S-parameters are presented in Fig. 5 and Fig. 6. The simulated peak gain of the LNA is 20.5dB at 80GHz and the 3-dB bandwidth is greater than 25GHz with upper 3-dB point falling after 94GHz. Input and output return losses remain <-9dB for the entirety of W-band, the reverse isolation is <-50dB for the same range. Fig. 7 shows the simulated NF of the LNA, the NF is below 6.2dB across the W-band, with the minimum value of 5.02dB at 93GHz. The simulated NF and NFmin are very close between 85-95 GHz range, indicating good noise

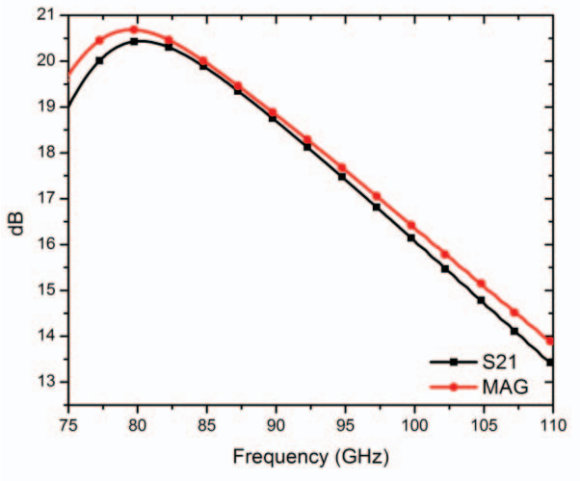

Fig. 5: Simulated gain vs. maximum gain of the LNA.

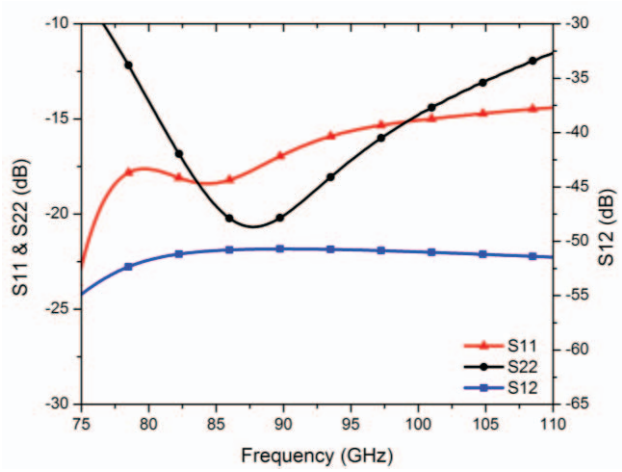

Fig. 6: Simulated input/output return losses and reverse isolation of the LNA.

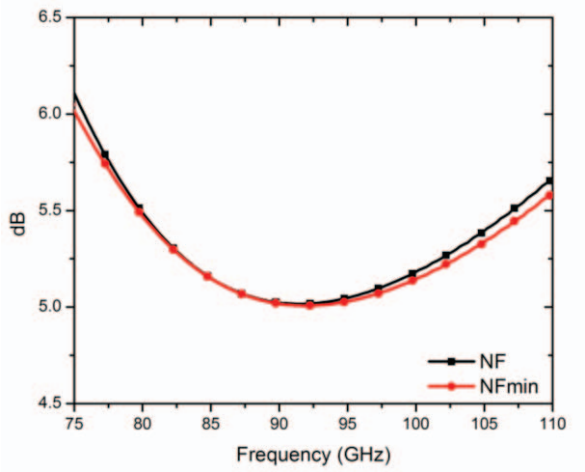

Fig. 7: Simulated NF and NFmin of the LNA.

matching. As shown in Fig. 8, LNA has an IP_{1dB} of -16dBm at 94 GHz which is more than enough for passive imagingapplications where the input signal power is significantly low.

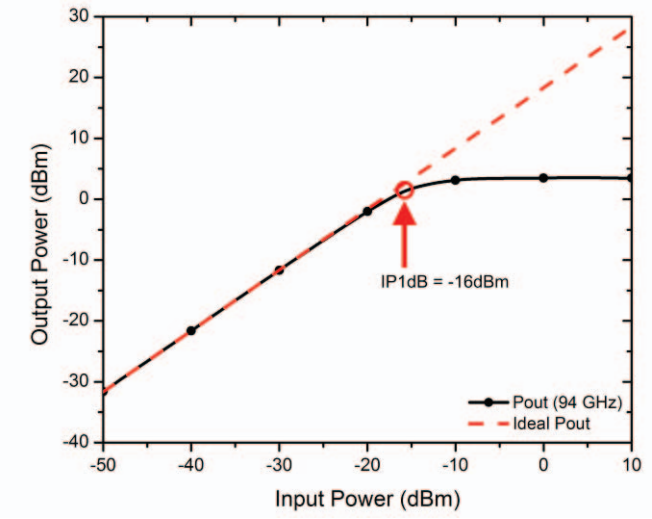

Fig. 8: Simulated 1-dB compression point at 94 GHz.

TABLE I
COMPARISON WITH PUBLISHED W-BAND SILICON LNAS

Ref.	Tech.	Peak Gain (dB)	3-dB BW (GHz)	NF (dB)	P_{DC} (mW)	Area (mm^2)
[10]	0.18µm SiGe	17	19	8	25.2	0.3
[13]	65nm CMOS	20	22	6.8-10	21	0.45
[14]	0.18µm SiGe	27	19	8.5	35	1
[15]	90nm SiGe	19	30	5.1	43	0.14*
This**	0.13µm SiGe	20.5	25	5	16	0.2*

*without pads **simulation

IV. CONCLUSION

In this paper, the design of a W-band low-noise amplifier using IHP's 0.13µm SiGe BiCMOS process for passive imaging systems has been presented. The simulation results show that the amplifier satisfies the specifications necessary to be used as a sub-block in a radiometer front-end system that can achieve <0.5K NETD. The use of inductors in the matching networks and inter-stages allowed a significant reduction in the overall chip area. Also, as seen from Table I, the LNA is comparable to the state-of-the-art in terms of performance with a moderate gain and good NF along with small chip area.

REFERENCES

[1] J. W. May and G. M. Rebeiz, "Design and Characterization of W -Band SiGe RFICs for Passive Millimeter-Wave Imaging," IEEE Transactions on Microwave Theory and Techniques, vol. 58, pp. 1420–1430, May 2010.

[2] S. T. Nicolson et al., "A Low-Voltage SiGe BiCMOS 77-GHz Automotive Radar Chipset," in IEEE Transactions on Microwave Theory and Techniques, vol. 56, no. 5, pp. 1092-1104, May 2008.

[3] I. Sarkas et al., "An 18-Gb/s, Direct QPSK Modulation SiGe BiCMOS Transceiver for Last Mile Links in the 70–80 GHz Band," in IEEE Journal of Solid-State Circuits, vol. 45, no. 10, pp. 1968-1980, Oct. 2010.

[4] F. Ulaby, R. Moore, and A. Fung, "Microwave remote sensing fundamentals and radiometry," in Microwave Remote Sensing: Active and Passive. Norwood, MA: Artech House, 1991.

[5] R. H. Dicke, "The measurement of thermal radiation frequencies," Revieww of Scientific Instruments, vol. 17, pp. 268–275, 1946.

[6] F. Thomsen, "On the Resolution of Dicke-Type Radiometers," IEEE Transactions on Microwave Theory and Techniques, vol. 32, pp. 145–150, Feb 1984.

[7] P. J. Rice, M. Black, D. Li, J. Yip, and J. McNicol, "Development of a low cost 94ghz imaging receiver using multilayer Liquid Crystal Polymer technology," in Physics and Engineering of Microwaves, Millimeter and Submillimeter Waves (MSMW), 2010 International Kharkov Symposium on, pp. 1–1, June 2010.

[8] R. L. Schmid, P. Song, C. T. Coen, A. . Ulusoy, and J. D. Cressler, "On the Analysis and Design of Low-Loss Single-Pole Double-Throw W-Band Switches Utilizing Saturated SiGe HBTs," IEEE Transactions on Microwave Theory and Techniques, vol. 62, pp. 2755–2767, Nov 2014.

[9] L. Zheng, L. Gilreath, V. Jain, and P. Heydari, "Design and analysis of a W-Band detector in 0.18- µm SiGe BiCMOS," in Silicon Monolithic Integrated Circuits in RF Systems (SiRF), 2010 Topical Meeting on, pp. 196–199, Jan 2010.

[10] R. Jonsson, R. Malmqvist, S. Reyaz, A. Rydberg, and M. Kaynak, "Design and results of W-band power detectors in a 130 nm SiGe BiCMOS process technology," in European Microwave Integrated Circuit Conference (EuMIC), 2014 9th, pp. 289–292, Oct 2014.

[11] S. T. Nicolson and S. P. Voinigescu, "Methodology for Simultaneous Noise and Impedance Matching in W-Band LNAs," 2006 IEEE Compound Semiconductor Integrated Circuit Symposium, San Antonio, TX, 2006, pp. 279-282.

[12] H. Rücker, B. Heinemann, and A. Fox, "Half-terahertz SiGe BiCMOS technology," in Proc. IEEE Silicon Monolithic Integr. Circuits RF Syst., Jan. 2012, pp. 133–136.

[13] C. J. Lee, H. J. Lee, J. G. Lee, T. H. Jang and C. S. Park, "A W-band CMOS low power wideband low noise amplifier with 22 dB gain and 3dB bandwidth of 20 GHz," 2015 Asia-Pacific Microwave Conference (APMC), Nanjing, 2015, pp. 1-3.

[14] L. Gilreath, V. Jam, and P. Heydari, "A W-band LNA in 0.18- µm SiGe BiCMOS," in Proceedings of 2010 IEEE International Symposium on Circuits and Systems, pp. 753–756, May 2010.

[15] Y. Yang, S. Cacina and G. M. Rebeiz, "A SiGe BiCMOS W-Band LNA with 5.1 dB NF at 90 GHz," *2013 IEEE Compound Semiconductor Integrated Circuit Symposium (CSICS)*, Monterey, CA, 2013, pp. 1-4.